CYBERNETICS AND PHYSICS, VOL. 10, NO. 2, 2021, 63–74

BIDIRECTIONAL CONTROLLED MULTIPLE SYNCHRONIZATION OF UNBALANCED ROTORS AND ITS EXPERIMENTAL EVALUATION

Boris Andrievsky
Inst. Problems Mechanical Engg.,
Russian Acad. of Sciences;
Saint Petersburg State University
Saint Petersburg, Russia
boris.andrievsky@gmail.com

Vladimir I. Boikov
ITMO University
Saint Petersburg, Russia
viboikov@mail.ru

Abstract
In the paper the problem of multiple controlled synchronization of a pair of unbalanced rotors is considered. A new bidirectional control law is proposed for multiple synchronization of rotors. A linear analysis of the dynamics of a simplified system model is presented, demonstrating the control system robustness with respect to the parameters of the vibration machine and controller. The main part of the paper is devoted to the description of the experimental results obtained at the Multiresonance Mechatronic Laboratory Setup, demonstrating the efficiency of the proposed approach and revealing its application scope.

Key words
phase shift, vibration machine, control, multiple synchronization, robustness

1 Introduction

In the development of vibratory machines that perform screening, crushing, vibration transportation of bulk materials, the increase in productivity is largely associated with the solution of the problem of ensuring a stable synchronous mode. The present paper is devoted to the problem of multiple controlled synchronization of a pair of unbalanced rotors. A new law of bidirectional control is proposed for multiple synchronization of rotors. A linear analysis of the dynamics of a simplified system is presented, demonstrating the robustness of the control system with respect to the parameters of the vibration machine and the controller. The main part of the paper gives a description of the experimental results obtained at the Multi-resonance Mechatronic Laboratory Setup, demonstrating the efficiency of the proposed approach and revealing its application area. The foundations of the theory of synchronization of vibration machines were laid in the 1960s in the works by I.I. Blekhman, where the basics of the theory of mechanical vibro-exciters synchronization were established, see (Blekhman, 1988; Blekhman *et al.*, 1995; Blekhman *et al.*, 1997; Blekhman, 2000; Blekhman, 2013; Blekhman *et al.*, 2002; Blekhman and Fradkov, 2004; Blekhman and Yaroshevich, 2004; Blekhman and Vaisberg, 2011; Blekhman, 2012). Based on this theory, the synchronization machinery of traditional rigid transmission (e.g., gear transmission) and flexible transmission (e.g., chain or belt transmission) are gradually reduced, replaced by vibration synchronization equipment driven by two or more exciters. They enable the vibrating system to achieve linear motion trajectory, elliptical motion trajectory and other kinds of nonlinear trajectories through vibrating synchronization (Li and Chen, 2019). The application of this theory made the work of synchronous machines extremely simple, making the maintenance easy and convenient and significantly improving the reliability of these machines. Moreover, as shown in these works, in many cases, synchronization in vibration devices is achieved due to the effect of self-synchronization of rotating rotors. In (Kremer, 2016) the method of direct separation of motions proposed by I.I. Blekhman was applied in a modified form with the explicit introduction of a small parameter. Equations for the slow motions were obtained and an analysis of how they depend on the structure of the original equations was performed. As an example, in (Kremer, 2016) is shown that high-frequency excitation in a system with a nonlinear friction can essentially increase the effective damping.

In (Li and Chen, 2019), *Li and Chen* analyzed the principle of operation of an elliptical vibration screening system driven by two motors and suggested adding a high frequency, low amplitude exciter at the end of the discharge, reducing screen clogging and separating the granular particles of the viscous block quickly and efficiently. Steady-state phase relationships for double frequency synchronization of vibration are ob-

tained and a functional relationship is given, according to which the location and direction of rotation of the exciters affect the phase difference between the actuators. Experimental results from (Li and Chen, 2019) have shown that synchronization of multi-frequency oscillations with three exciters can be achieved.

The phenomenon of vibration synchronization of a two-mass oscillatory system driven by two actuators was studied in (Liu *et al.*, 2020). The averaging method was used for deriving a criterion for synchronization between two actuators as well as a criterion for the stability of an oscillatory system in synchronous states is given. The rotation speed of the two actuators, the phase difference between their rotation angles, responses and the difference in responses of two solids were studied quantitatively in the subresonant and superresonant states of the system, as well as on a technical example of vibration synchronization of a two-mass vibrational system, driven by two actuators, was presented.

In a number of cases, however, the self-synchronization effect is not stable enough, and can also hinder the achievement of the desired behavior of the system, for example, when it is necessary to provide specified phase shifts between the rotors or to provide a multiple synchronization mode. In these cases, the solution can be to use closed-loop control for vibration machines. Let us consider some results of this approach. A synchronization control strategy for the multi-motor control system using the MS (Master-Slave) communication mode, based on the PROFIBUS-DP fieldbus (Vitturi, 2004), was proposed by *He et al.* in (He *et al.*, 2007). In order to properly assign the given speed of each motor of the slave station, the arithmetic neural network controller was installed on the master station.

In (Tomchina *et al.*, 2009; Galitskaya and Tomchina, 2012; Tomchina, 2020), a multiple synchronization algorithm for a two-rotor vibration machine is proposed, based on the integro-differentiating Speed-gradient algorithms (Fradkov, 1979; Andrievsky *et al.*, 1989; Fradkov and Pogromsky, 1998; Fradkov *et al.*, 1999). It is shown that the proposed solution to the problem of controlling the multiple synchronization of rotors of two-rotor vibration machines affects the value of the steady-state normalized phase shift, making it possible to regulate the performance of the system. The results of computer simulation are presented, which confirm the effectiveness of the developed algorithm.

In (Jia *et al.*, 2018), the master-slave control strategy was employed to realize the multi-frequency synchronization. To this end, the fuzzy PID method is used to control two induction motors. The slave motor uses the method of the phase ratio to trace the master motor and achieve the synchronous motion. The motion trails of the vibrating system between one and two times and realizes the zero phase difference after each period. The experiments are used to analyzing the feature of the movement tracks. In the experiment of the multi-frequency controlled synchronization, the speeds of the two motors are, respectively, set to 27 Hz and 40.5 Hz with two inverters. The PLC (Programmable Logic Controller) was used to realize the master-slave control strategy. The photoelectric coder and the Hall sensor are used to measure and calculate the pulses.

In the present paper a novel bidirectional control law for multiple synchronization of the pair of debalance rotors is proposed. A linear analysis of the dynamics of a simplified system is presented, demonstrating the robustness of the control system with respect to the parameters of the vibration machine and the controller. The main part of the paper contains description of the experimental results obtained at the Multi-resonance Mechatronic Laboratory Setup, demonstrating the efficiency of the proposed approach and revealing its application area.

The reminder of the paper is organized as follows. The Mechatronic Setup SV-2M for performing the experiments is briefly described in Sec. 2. Section 3 presents the bidirectional control law for multiple synchronization of the debalance rotors. Linear analysis of the simplified closed-loop system is given in Sec. 4. Results of the experiments are presented in Sec. 5. Concluding remarks and the future work intentions are given in Sec. 6.

2 Description of Experimental Mechatronic Setup

The Multiresonance Mechatronic Laboratory Setup (MMLS) SV-2M of the IPME RAS, described in (Boikov *et al.*, 2016; Fradkov *et al.*, 2016; Andrievsky and Boikov, 2017; Andrievsky *et al.*, 2019; Fradkov *et al.*, 2021), is used for experimental investigations. For the sake of clearness, the SV-2M is briefly described below.

The MMLS SV-2M was developed on the basis of many years of experience on creating vibrating stands at the Mekhanobr Engineering JSC and the IPME RAS. Professor I.I. Blekhman was among the initiators of the development of the stand, he outlined the range of its possible applications in research works on vibration technologies, the mechanical resonance phenomena and oscillations synchronization. I.I. Blekhman had paid the great attention to the works performed on the setup, actively participated in the discussion, helped interpretation of experimental results and had suggested the directions for further research, cf. (Andrievskii *et al.*, 2016).

The mechatronic setup SV-2M consists of the *vibration stand*, a pair of the *induction motors* with *unbalanced rotors*, the *electronic converter/amplifier*, the *sensor assembly* with the special *controller* for signal processing, and the *personal computer*, supplied with the devices for interface with the hardware. The AC

Figure 1. General view of the mechatronic setup SV-2M.

motors can be independently controlled by means of the control signals, computed by the PC and applied to the corresponding amplifier. Unbalance of the rotors is provided by the eccentrically located weight. The unbalanced rotor rotates on the motor shaft in a vertical plane on the stand base. Upon rotation of the unbalanced rotors around their axes, the centrifugal forces arise, which excite vibrations in positions of the spring-loaded main platform and the additional platform.

The general view of the setup, including the electronics assembly box, the PC and the vibration stand (from left to right) is depicted in Fig. 1. Notations on the figure: 1 – AC induction motor; 2 – drive shaft; 3 – unbalanced rotor; 4 – base; 5 – springs of the main platform; 6 – additional platform; 7 – springs of the additional platform. The mechanical part of the setup is pictured in Fig. 2 in more details. The rotors' revolving directions are not controlled in SV-2M. The positive direction for the "left" (conventionally) motor is clockwise, whereas for the "right" motor it is anti-clockwise.

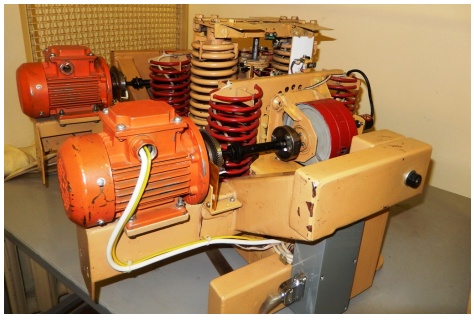

Figure 2. Mechanical part of the mechatronic setup SV-2M.

The stand is equipped with 12 optical sensors measuring positions of the main and of the extra platforms, velocity sensors for two independently rotating rotors, having a resolution of 4000 pulses/revolution, as well as with the sensors of electric motor currents. Measurement of the platforms positions is carried out by a set of sensors. First of all, these are optical motion sensors, installed in such a way that their data allow obtaining information about the 6DoF linear and angular coordinates of each platform. To this end, the *DFRobot Smart Grayscale Sensors* are employed. In the SV-2M, the analog sensor output is used, which is fed to the analog I/O board *PCI826* for transferring measured data to the PC. The drive systems are independently controlled from the main *personal computer* (PC), which forms the governing signals u_l and u_r setting the drive rotation speed of the "left" and "right" drive system (respectively). These signals are applied to *Altivar 12 Schneider Electric* converters over the 16-bit DAC in the form of the DC voltages, which lie the interval $[0, 5]$ V. The converters have their local feedback, used in the "$U/f = \text{const}$" controlling mode. The PC outputs are integers from the range $[0, 2^{16} - 1]$. Therefore, the dimensionless control signals, formed by the PC, are non-negative and are limited by $\bar{u} = 65535$.

Real-time data processing and control are carried out by means of Simulink Desktop Real-Time™ of MATLAB© R2015b software. Control signal computation can be performed with a sampling rate up to 1000 Hz.

3 Bidirectional Control Law for Multiple Synchronization of Debalance Rotors

In (Andrievsky *et al.*, 2019; Fradkov *et al.*, 2021) the problem of controlled synchronization for unbalanced rotors phase shift is considered. The rotation frequency band is conditionally partitioned into the following ranges:

1. *ultra-low frequencies*: $0 \leqslant \omega < 30$ rad/s;
2. *low frequencies*: $30 \leqslant \omega < 50$ rad/s;
3. *medium frequencies*: $50 \leqslant \omega < 70$ rad/s;
4. *high frequencies*: $70 \leqslant \omega < 100$ rad/s;
5. *superior frequencies*: $\omega \geqslant 100$ rad/s.

At frequency $\omega \approx 125$ rad/s the Sommerfeld effect (Sommerfeld, 1902; Blekhman, 1988; Dimentberg *et al.*, 1997; Blekhman and Fradkov, 2004; Kovriguine, 2012; Cvetićanin and Zukovic, 2015) manifests itself; the frequencies in this range and the upper one have not been experimentally studied in (Andrievsky *et al.*, 2019; Fradkov *et al.*, 2021) and are not considered in the present study.

The control laws for frequency stabilization along with the prescribed phase shift between the rotors angular positions are proposed and experimentally studied on the mechatronic vibration setup SV-2M. It is obtained that for the low and medium frequencies the self-synchronization of unbalanced rotors does not prevent ensuring the desired phase shift between the rotors. For a high frequency band, the Huygens self-synchronization of rotors manifests itself, narrowing the range of the achievable phase shift. Nevertheless for all the frequencies less than the frequency of the Sommerfeld effect, the desired phase shift in the range of $\pm\pi/2$ rad can be ensured.

The investigations of (Andrievsky *et al.*, 2019) were continued in (Fradkov *et al.*, 2021), where the problem of synthesis and analysis of vibration fields is con-

sidered and it is shown that the vibration field of the two-rotor vibration system depends on the coordinates of the points of fastening of the rotors, the mass of the debalances and the steady phase difference of the debalances provided they are in stable synchronous rotation mode. The control law of (Andrievsky *et al.*, 2019; Fradkov *et al.*, 2021) is of a bidirectional form, where the rotation velocity of each actuator is controlled independently of the other one by means of its separated PI-controller with adding the symmetrical cross-coupling between the control loops, produced by the joint phase-shift PI-controller. The control law of (Andrievsky *et al.*, 2019; Fradkov *et al.*, 2021) is borrowed in the present paper aiming to produce the multiple synchronization of the rotors with a given normalized phase shift ψ^*. To this end the *normalization gain* $\kappa > 0$ is introduced, so that the desired rotation frequencies of the left ω_l^* and right ω_r^* rotors are related as $\omega_r^* = \omega_l^*/\kappa$ and, consequently, the normalized phase shift ψ between the rotors is calculated as $\psi = \kappa\varphi_r - \varphi_l$, cf. (Tomchina *et al.*, 2009; Galitskaya and Tomchina, 2012; Tomchina, 2020).

Summarizing, the adopted bidirectional control law for multiple synchronization of debalance rotors is as follows:

$$\omega_r^* = \kappa^{-1}\omega_l^*, \tag{1}$$
$$e_{\omega_l} = \omega_l^* - \omega_l, \quad e_{\omega_r} = \omega_r^* - \omega_r, \tag{2}$$
$$\dot\sigma_{\omega l} = e_{\omega_l}, \quad u_{\omega_l} = K_{i\omega_l}\sigma_{\omega l} + K_{p\omega_l}e_{\omega_l}, \tag{3}$$
$$\dot\sigma_{\omega r} = e_{\omega_r}, \quad u_{\omega_r} = K_{i\omega_r}\sigma_{\omega r} + K_{p}e_{\omega_r}, \tag{4}$$
$$\psi = \kappa\varphi_r - \varphi_l, \tag{5}$$
$$e_\psi = \psi^* - \psi, \tag{6}$$
$$\dot\sigma_\psi = \sin e_\psi, \quad u_\psi = -K_{i,\psi}\sigma_\psi + K_{p,\psi}\sin e_\psi, \tag{7}$$
$$u_l = u_{\omega_l} + u_\psi, \quad u_r = u_{\omega_r} - u_\psi, \tag{8}$$

where ω_r^*, ω_l^* denote the reference values for left and right motor velocities, κ stands for the normalization coefficient; e_{ω_l}, e_{ω_r} are the motor velocity errors; PI-controllers for velocities of the left and right motors are described by (3), (4), respectively, where $K_{i\omega_l}$, $K_{i\omega_r}$ are for the integral, and $K_{p\omega_l}$, $K_{p\omega_r}$ are for the proportional controller gains; in (5), φ_r and φ_l denote the phase angles of the rotors, ψ stands for the normalized phase shift between the rotors; the phase shift error is denoted by e_ψ, where ψ^* is the prescribed phase shift between the rotors; (7) describes the phase shift PI-controller (following (Andrievsky *et al.*, 2019; Fradkov *et al.*, 2021), its *sine-modification* is used); u_l and u_r in (8) denote the control signals applied to the left and right drive systems. It is worth mentioning that, since the difference in the integer number of rotor revolutions is insignificant, instead of the sine-modification, it is possible to reset the readings of the rotor angular sensors at the end of each full rotor turnover.

4 Linear Analysis of Simplified Model

The overall system, including the mechanical part, induction motors and the controller is a highly nonlinear complex system of the high order (cf. (Galitskaya and Tomchina, 2012; Fradkov *et al.*, 2013; Tomchina, 2018; Tomchina, 2020; Fradkov *et al.*, 2021)). However, as stated in (Fradkov *et al.*, 2021), in medium and high frequency ranges, the so-called the *averaging property*, which is widely exploited in the vibrational mechanics is valid. Due to this property, the fast oscillating components are averaged and only the "slow" motions may be taken into account, see (Blekhman, 1988; Blekhman, 2000; Kremer, 2016). What is more, since the induction motors have their local feedback controllers, the dynamics of the drive systems, including the induction motor, the frequency converter with the feedback local controller may be approximately described by the following transfer function from control signal u to angular velocity ω, cf. (Khalil *et al.*, 2009; Joshi and Chandorkar, 2014; Giri, 2013; Fradkov *et al.*, 2021):

$$W_d(s) = \left\{\frac{\omega}{u}\right\} = \frac{K_d}{(T_1 s + 1)(T_2 s + 1)}, \tag{9}$$

where K_d denotes the drive system static gain; T_1 and T_2 are time constants (parameters K_d, T_1, T_2 may differ for the left and the right drives; in this case they are labeled by the corresponding indeces "l" and "r"); $s \in \mathbb{C}$ is the Laplace transform variable. For drive model parameters identification the standard non-recursive least-square estimation (LSE) method was employed in (Ljung, 1999; Andrievsky *et al.*, 2016). The results of the identification procedure for various ω_0 demonstrated that the variations of the drive system model (9) parameters for different regions of the operating frequency are small and the "averaged" values $K_d = 0.041$ rad/s, $T_1 = 1.75$ s, $T_2 = 0.246$ s for both drives are taken.

Model (9) and its parameters are used in this work for the linear analysis of the simplified system. Also, for the linear analysis of this Section, boundedness of the drive input signals u_l, u_r is ignored, assuming that it makes an effect during the start-up mode only, not at the nominal operation regime and the sine-modification (7) is replaced by the following linear equation

$$\dot\sigma_\psi = e_\psi, \quad u_\psi = -K_{i,\psi}\sigma_\psi + K_{p,\psi}e_\psi. \tag{10}$$

These assumptions validation is made experimentally in Sec. 5.

For studying the system stability let us employ the frequency (Nyquist) criterion. To this end let us derive the open-loop system transfer function, breaking the connection in the phase shift control loop, and considering signal u_ψ as the input of the open-loop system and

Table 1. Stability Margins G_m, P_m and ω_{cg}, ω_{cp}

κ	G_m, dB	ω_{cg}, rad/s	P_m, deg	ω_{cp} rad/s
0.5	12.1	3.3	58.4	1.05
1.0	9.57	3.3	52.3	1.36
2.0	6.05	3.3	37.7	2.0

the output $y = K_{i,\psi}\sigma_\psi + K_{p,\psi}e_\psi$ of the phase shift PI-controller (10) as an output of the open-loop system. Further, let us denote the transfer functions of the closed-loop systems from input u_ψ to outputs ω_l, ω_r (described by Eqs. (2) – (4), (9)) as $W_{\omega,l}(s)$ and $W_{\omega_r}(s)$ for the left and the right drives, respectively. Then, taking into account relations $\dot\varphi_l = \omega_l$, $\dot\varphi_r = \omega_r$, relation for the open-loop system output y and Eqs. (5), (6), one obtains the following transfer function of the open-loop system

$$W(s) = \frac{K_{p,\psi}s + K_{i,\psi}}{s^2}\big(W_{\omega,l}(s) + \kappa W_{\omega,r}(s)\big). \quad (11)$$

Let us mention, that the Nyquist criterion can be also applied directly to the MIMO system (2) – (4), (9), as it proposed in (Bucolo *et al.*, 2022).

Direct calculations lead to the following transfer functions $W_{\omega,l}(s)$, $W_{\omega,r}(s)$:

$$W_{\omega,\{lr\}}(s) = \frac{K_{d,\{lr\}}s}{A_{\omega,\{lr\}}(s)}, \quad \text{where} \quad (12)$$
$$A_{\omega,\{lr\}}(s) = T_{1,\{lr\}}T_{2,\{lr\}}s^3 + (T_{1,\{lr\}} + T_{2,\{lr\}})s^2 + (K_{d\{lr\}}K_{p,\omega\{lr\}} + 1)s + K_{d\{lr\}}K_{i,\omega\{lr\}}.$$

For numerical evaluation of the system dynamics, the following model parameters are taken: $K_{i,\omega r} = K_{i,\omega l} = 730$, $K_{p,\omega r} = K_{p,\omega l} = 1260$ s, $K_{p,\psi} = 760$, $K_{i,\psi} = 650$ s, $K_{dr} = K_{dl} = 0.0041$, $T_{1r} = T_{1l} = 1.7496$ s, $T_{2r} = T_{2l} = 0.2460$ s. The magnitude Bode plots for various $\kappa \in \{0.5, 1.0, 2.0\}$ are shown in Fig. 3, and the corresponding frequency stability margins for various κ are given in Tab. 1, where the following notation is used: the gain margin G_m, the phase margin P_m, the associated frequencies are ω_{cg}, ω_{cp}. (Gain and phase margins and the crossover frequencies are found with the help of MATLAB routine *margin*). It is seen that the margins are acceptable for practice save the case of $\kappa = 2.0$, where the gain margin $G_m = 6.05$ dB is a bit less the habitually recommended one as 7.6 dB. However, if necessary, it may be increased by decreasing overall PI-phase controller gain for large κ. It is worth mentioning, that κ is not changed rapidly during the system operation, and this correction may be easily done before starting the system. Alternatively, the adaptation methods can be used for adjusting the controller parameters.

Let us consider now the linearized model of the closed-loop system (1)–(6), (8), (9), (10) with inputs ω_l^*, ψ^* and outputs e_{ω_l}, e_{ω_r}, e_ψ. Defining input and output vectors as $u = [\omega_l^*, \psi^*]^{\mathrm{T}}$ and $y = [e_{\omega_l}, e_{\omega_r}, e_\psi]^{\mathrm{T}}$ on can represent (1)–(6), (8), (9) in the following vector-matrix form

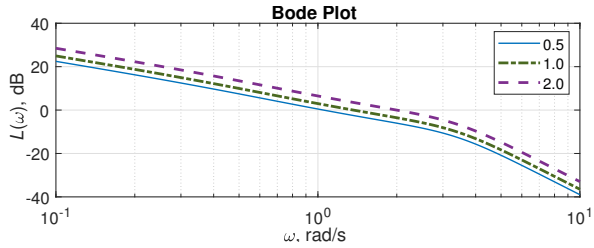

Figure 3. Bode Plots for $\kappa \in \{0.5, 1.0, 2.0\}$.

$$D(p)y(t) = R(p)u(t), \quad (13)$$

where $p = \mathrm{d}/\mathrm{d}t$ denotes the differential operator on time t, $D(s) = d_0 s^7 + \cdots + d_7$, $s \in \mathbb{C}$, is the Hurwits polynomial if the asymptotic stability conditions for the closed-loop system (13) are valid (in this case, $d_7 > 0$), and

$$R(p) = \begin{bmatrix} R^{e_{\omega_l}}_{\omega_l^*}(p) & R^{e_{\omega_l}}_{\psi^*}(p) \\ R^{e_{\omega_r}}_{\omega_l^*}(p) & R^{e_{\omega_r}}_{\psi^*}(p) \\ R^{e_\psi}_{\omega_l^*}(p) & R^{e_\psi}_{\psi^*}(p) \end{bmatrix}. \quad (14)$$

Consider the steady-state mode, assuming that the time derivatives in (3), (4), (10) are zeros. This leads to zero steady-state regulation errors, i.e. that it is valid for (13) that $R(0) = 0$. It should be stressed that this is a structural property of the system, which is robust with respect to the plant and controller parameters. robustness of the closed-loop system stability is demonstrated above with the help of the frequency stability criterion, see Fig. 3 and Tab. 1. More detailed information about the closed-loop linearized system dynamics for given above system parameters may be obtained from Figs. 4–7. Pole-zero locus of transfer functions $\Phi^{e_\psi}_{\psi^*}(s) = R^{e_\psi}_{\psi^*}(s)/D(s)$ and $\Phi^{e_{\omega_l}}_{\omega_l^*}(s) = R^{e_{\omega_l}}_{\omega_l^*}(s)/D(s)$ for the various values of $\kappa \in \{0.5, 1.0, 2.0\}$ are demonstrated in Figs. 4–6. Corresponding step responses are plotted in Fig. 7.

5 Experimental Results

The experimental study of the multiple synchronization by means of the control law (1)–(8) has been performed on the MMLS SV-2M for the set of desired frequencies ω_l^* covered the ultra-low, low, middle, low and high frequency ranges for various values of normalization coefficient κ and demanded normalized phase shift ψ^*.

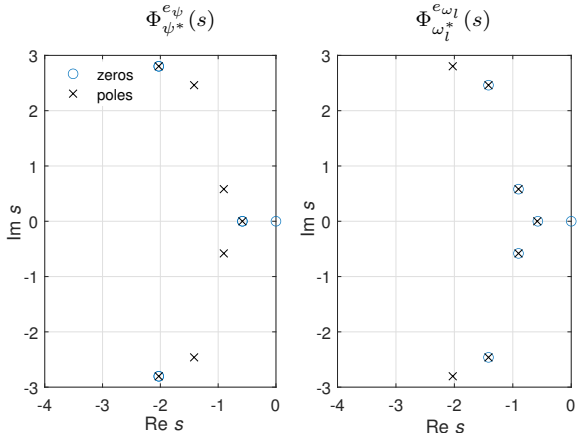

Figure 4. Pole-zero locus for $\kappa = 0.5$.

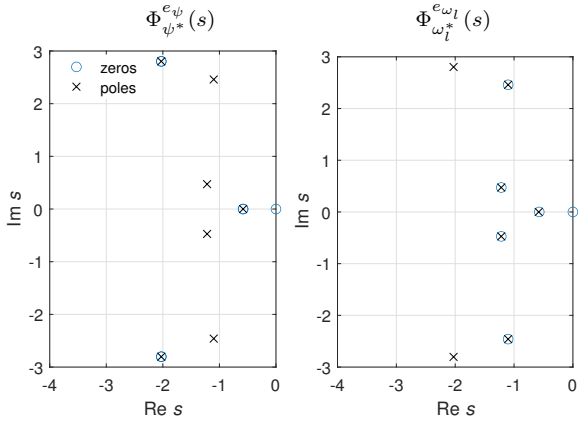

Figure 5. Pole-zero locus for $\kappa = 1.0$.

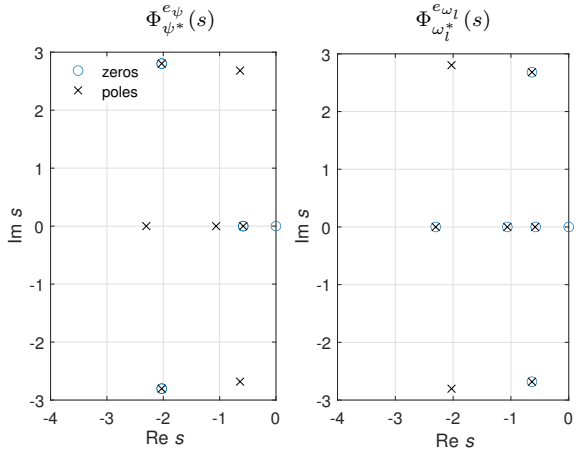

Figure 6. Pole-zero locus for $\kappa = 2.0$.

5.1 Experiments for Ultra-Low Frequency Range

The experimental results for the region of ultra-low frequencies are shown in Figs. 8–11. Figures 8, 9 refer to the desired rotation speed of both rotors ω_l^*, ω_r^* equal to 10 rad/s ($\kappa = 1$) and the desired synchronous

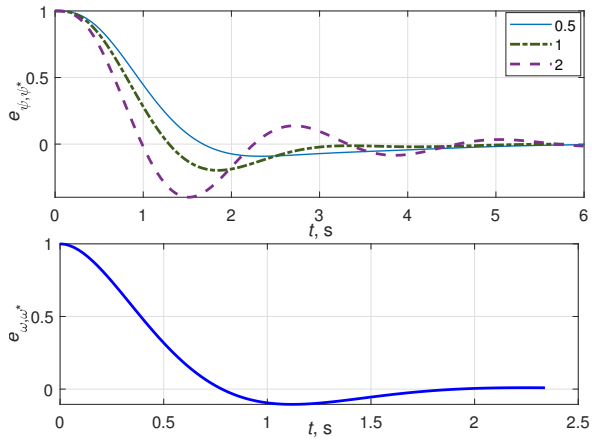

upper plot: $\Phi^{e_\psi}_{\psi^*}(s)$, lower plot: $\Phi^{e_{\omega_l}}_{\omega_l^*}(s)$

Figure 7. Step responses for $\kappa \in \{0.5, 1.0, 2.0\}$.

rotation of the rotors, i.e. $\psi^* = 0$.[1] The angular rotation velocities time histories are plotted in Fig. 8. The Lissajous curves in coordinates $(\sin\varphi_l, \sin\varphi_r)$ are depicted in Fig. 9. These plots may be treated as the trajectories of the rotors' corresponding points projections to the vertical axis.

As one can see from the results obtained, the "pendulum" torque arising from the unbalance of the rotors in this speed range has a significant effect on the rotation speed. This is due to the fact that the torque required by the engine to give rotation at the low speed is comparable to the torque of the gravitational forces, and the response rate of the drive is not enough for compensating gravitational disturbances. The Lissajous plot shown in Fig. 9 demonstrates that, despite the deviations in the angular rotation velocity, the required synchronous movement of the rotors is provided with acceptable accuracy. Note that the Lissajous plot corresponding to synchronous rotation represents by the bisector segment of the first and third quadrants.

The corresponding plots for angular velocities and Lissajous figures at $\omega_l = 30$ rad/s, $\kappa = 3$ (that is, $\omega_r = 10$ rad/s) and the demanded phase shift $\psi^* = \pi$ are depicted in Figs. 10, 11. The Lissajous curve on Fig. 11 corresponds to the "normalized" projections on the plane $\big(\sin\varphi_l, \sin(\kappa\varphi_r)\big)$. One can see that, in average, the required rotation speeds are also provided, but it is not possible to ensure the desired phase shift between the rotation angles: instead of a segment on the diagonal of the second and fourth quadrants, a complex Lissajous curve is obtained, as one can see from Fig. 11.

5.2 Experiments for Low Frequency Range

The low frequencies band has very limited bounds for multiple synchronization due to the significant impact of the debalance torques on the motor rotation

[1] Recall that in the MMLS SV-2M, clockwise rotation of the left rotor, and counterclockwise of the right one are considered positive.

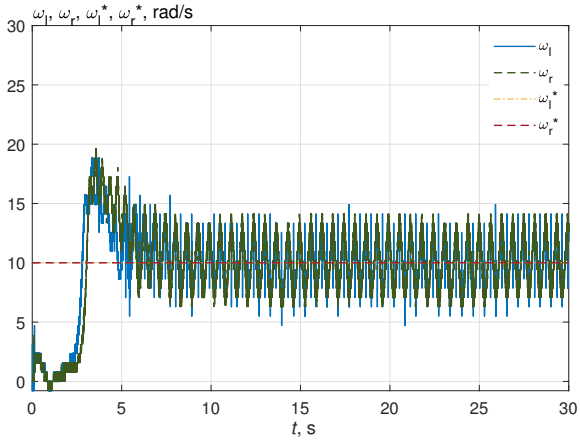

Figure 8. Time histories of the rotor angular velocities ω_l, ω_r. $\omega_l^* = 10$ rad/s, $\kappa = 1$, $\psi^* = 0$.

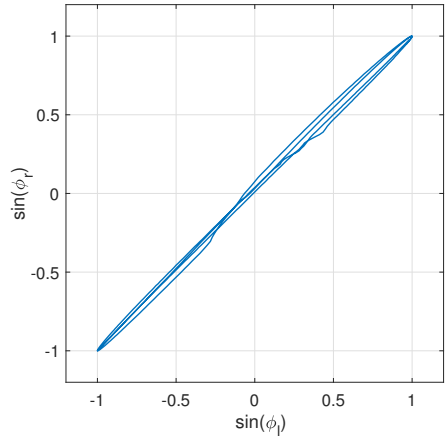

Figure 9. Lissajous Curves. $\omega_l^* = 10$ rad/s, $\kappa = 1$, $\psi^* = 0$.

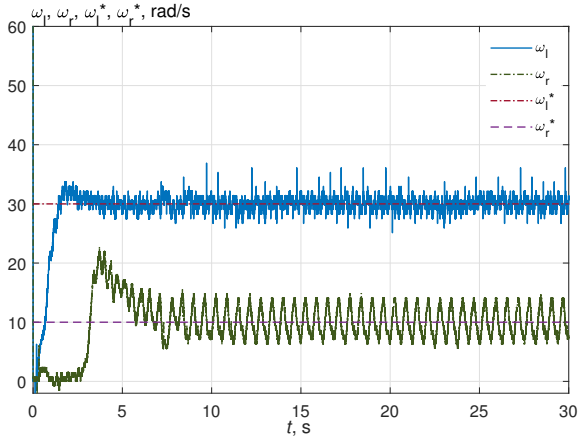

Figure 10. Time histories of the rotor angular velocities ω_l, ω_r. $\omega_l^* = 30$ rad/s, $\kappa = 3$, $\psi^* = \pi$.

and proximity to the lower resonant frequency of the main platform (cf. (Tomchin and Fradkov, 2005; Fradkov *et al.*, 2011; Gorlatov *et al.*, 2015; Fradkov *et al.*, 2016; Fradkov *et al.*, 2021)), therefore only a few experiments have been done in this frequency range. Results of the experiment are demonstrated by Figs. 12–14.

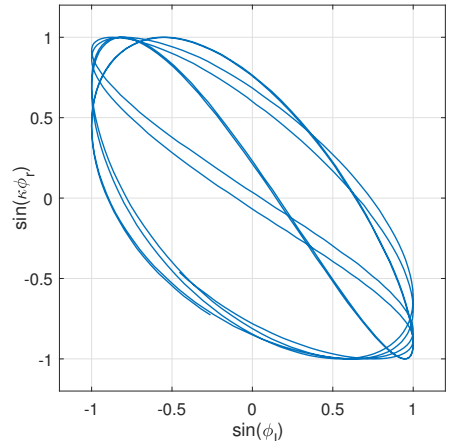

Figure 11. Lissajous Curves. $\omega_l^* = 30$ rad/s, $\kappa = 3$, $\psi^* = \pi$.

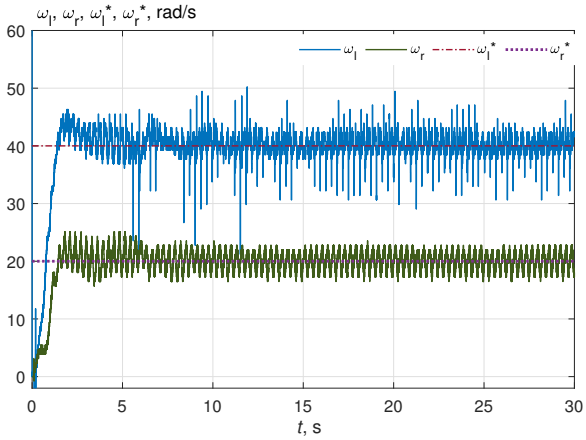

Figure 12. Time histories of the rotor angular velocities ω_l, ω_r. $\omega_l^* = 40$ rad/s, $\kappa = 2$, $\psi^* = \pi$.

The "basic" frequency $\omega_l^* = 40$ rad/s is picked out. The normalization parameter κ is taken as $\kappa = 2$, therefore ω_r^* is as $\omega_r^* = 20$ rad/s (and therefore lies in the ultra-low, "forbidden", frequency range). The desirable normalized phase shift is set to $\psi^* = \pi$. Time histories of the rotor angular velocities ω_l, ω_r are depicted in Fig. 12. As is seen from the plots, the averaged-values of the rotation speed are close to the desirable ones, however the noticeable bursts of rotation speed ω_l are observed, caused by the influence of the debalance torque and significant movements of the main platform. The time histories of $\sin\varphi_l$, $\sin(\kappa\varphi_r)$ and the desired process $\sin(\kappa\varphi_r^*)$, plotted in Fig. 13 and the Lissajous curves depicted in Fig. 14 show the notable phase shift error, which under certain circumstances, however, can be acceptable for practice. It is also worth mentioning that the low frequency range usually is not typical for the vibration technology needs.

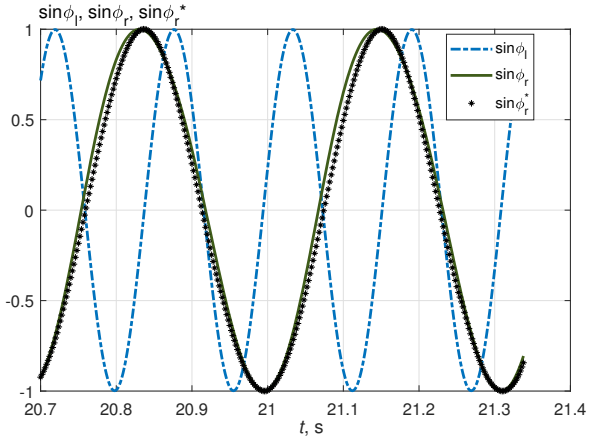

Figure 13. Time histories of $\sin\varphi_l$, $\sin\varphi_r$ and desired process $\sin\varphi_r^*$ for $\omega_l^* = 40$ rad/s, $\kappa = 2$, $\psi^* = \pi$.

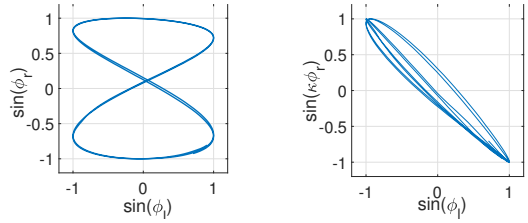

Figure 14. Lissajous Curves. $\omega_l^* = 40$ rad/s, $\kappa = 2$, $\psi^* = \pi$. Left: (φ_l, φ_r), right: $(\varphi_l, \kappa\varphi_r)$.

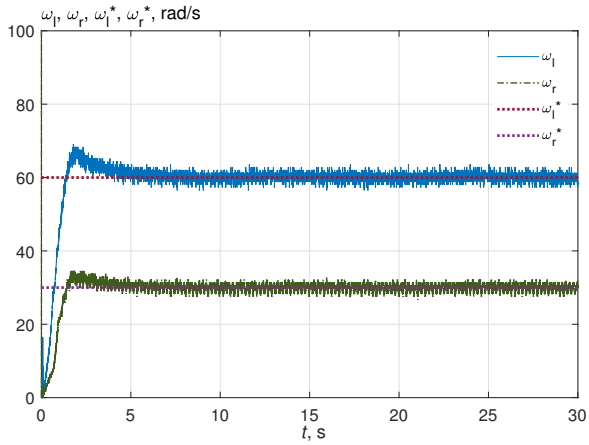

Figure 15. Time histories of the rotor angular velocities ω_l, ω_r. $\omega_l^* = 60$ rad/s, $\kappa = 2.0$, $\psi^* = 0$.

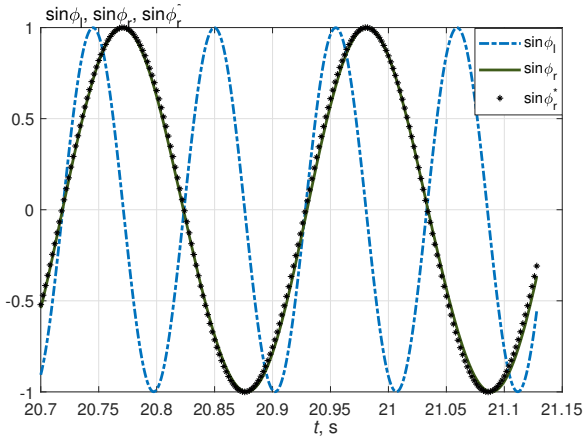

Figure 16. Time histories of $\sin\varphi_l$, $\sin\varphi_r$ and desired process $\sin\varphi_r^*$ for $\omega_l^* = 60$ rad/s, $\kappa = 2.0$, $\psi^* = 0$.

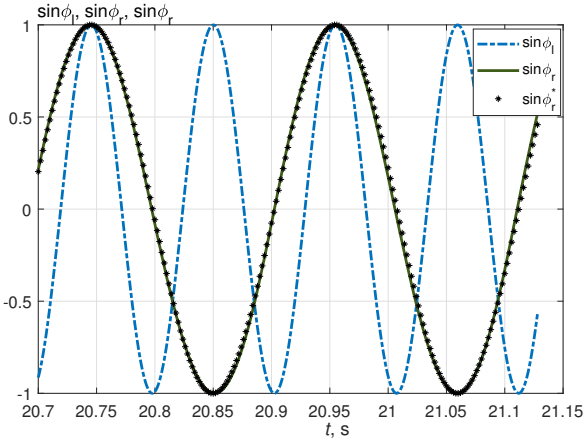

Figure 17. Time histories of $\sin\varphi_l$, $\sin\varphi_r$ and desired process $\sin\varphi_r^*$ for $\omega_l^* = 60$ rad/s, $\kappa = 2.0$, $\psi^* = \pi/2$.

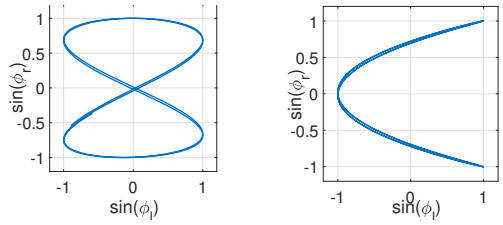

Figure 18. Lissajous Curves. $\omega_l^* = 60$ rad/s, $\kappa = 2.0$. Left: $\psi^* = 0$, right: $\psi^* = \pi/2$.

5.3 Experiments for Middle Frequency Range

Experimental results for the middle frequency range are depicted in Figs. 15–21.

Figures 15–18 are related to the case of $\omega_l^* = 60$ rad/s, $\kappa = 2$ (which means that $\omega_r^* = 30$ rad/s). Firstly, $\psi^* = 0$ is set. Time histories of the rotor angular velocities ω_l, ω_r for this case are shown in Fig. 15. It is seen that after the transient time lasting about 5 s, the prescribed frequencies are achieved. Figure 16 demonstrates achievement of the desired normalized phase shift between the rotors. In this figure, the time histories of $\sin\varphi_l$, $\sin\varphi_r$ and of the desired process $\sin\varphi_r^*$ are plotted. These curves may be treated as the projections of the certain points on the left and right rotors to the vertical axis during revolving. One can observe coincidence of the curves of $\sin\varphi_r$ and $\sin\varphi_r^*$ with a high accuracy. The corresponding time histories, but for $\psi^* = \pi/2$, are depicted in Fig. 17, where achievement of the prescribed multiple synchronization is also demonstrated. The plots in Fig. 18 show Lis-

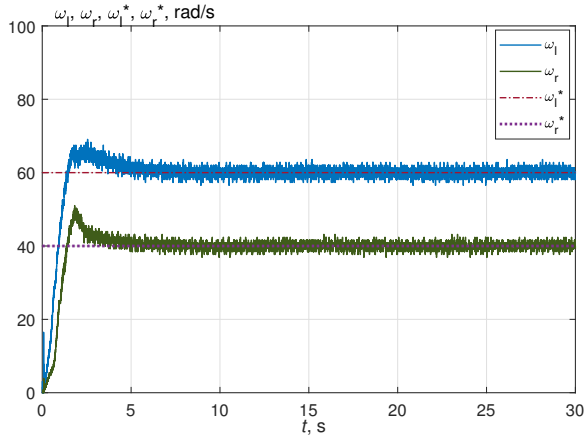

Figure 19. Time histories of the rotor angular velocities ω_l, ω_r. $\omega_l^* = 60$ rad/s, $\kappa = 3/2$, $\psi^* = \pi/2$.

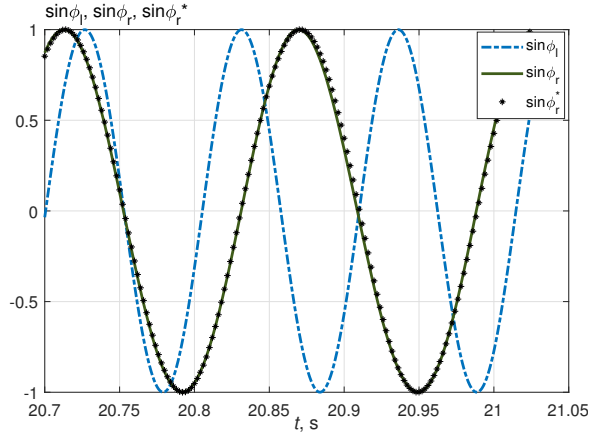

Figure 20. Time histories of $\sin\varphi_l$, $\sin\varphi_r$ and desired process $\sin\varphi_r^*$ for $\omega_l^* = 60$ rad/s, $\kappa = 3/2$, $\psi^* = \pi/2$.

sajous curves on the plane $(\sin\varphi_l, \sin\varphi_r)$ for the cases of $\psi^* = 0$ and $\psi^* = \pi/2$.

The experimental results for $\omega_l^* = 60$ rad/s, $\kappa = 3/2$ ($\omega_r^* = 40$ rad/s) and $\psi^* = \pi/2$ are presented in Figs. 19–21. Time histories of the rotor angular velocities ω_l, ω_r are shown in Fig. 19, demonstrating achievement of the desired rotation rates approximately after 4.5 s. Ensuring the demanded normalized phase shift between the rotors is seen from Fig. 20, where the time histories of $\sin\varphi_l$, $\sin\varphi_r$ and of the desired process $\sin\varphi_r^*$ are depicted. As well as in the above case of $\kappa = 2$, the precise regulation of the phase shift is observed. Some additional information about the system properties can be found from the Lissajous curves, plotted in Fig. 21. $\omega_l^* = 60$ rad/s, $\kappa = 3/2$, $\psi^* = \pi/2$. As above, the left curve demonstrates "real" projections of the certain points on rotors to the vertical axes as $(\sin\varphi_l, \sin\varphi_r)$, the right curve corresponds the "normalized" projections on the plane $\big(\sin\varphi_l, \sin(\kappa\varphi_r)\big)$. The given normalized phase shift as $\pi/2$ would be represented by means of the circle on the right plot.

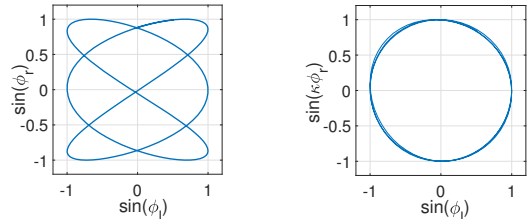

Figure 21. Lissajous Curves. $\omega_l^* = 60$ rad/s, $\kappa = 3/2$, $\psi^* = \pi/2$. Left: (φ_l, φ_r), right: $(\varphi_l, \kappa\varphi_r)$.

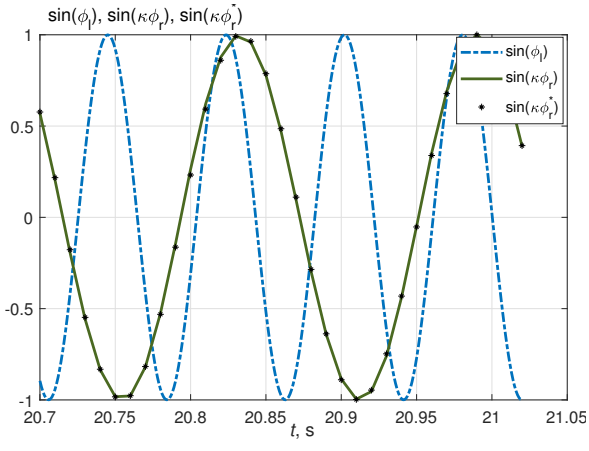

Figure 22. Time histories of $\sin\varphi_l$, $\sin(\kappa\varphi_r)$ and desired process $\sin(\kappa\varphi_r^*)$ for $\omega_l^* = 80$ rad/s, $\kappa = 2$, $\psi^* = \pi/2$.

5.4 Experiments for High Frequency Range

As was disclosed in (Andrievsky *et al.*, 2019; Fradkov *et al.*, 2021), in the high frequency range (and above) the self-synchronization property of the vibrating machine can overwhelm the efforts of the controller to ensure the desired phase shift between the revolving rotors. The experiments were made to check this feature for the multiple synchronization case. Some results are shown in Figs. 22, 24. Parameter $\kappa = 2$ was taken and ψ^* was set to $\psi^* = \pi/2$ for both experiments. Time histories of $\sin\varphi_l$, $\sin\varphi_r$ and desired process $\sin\varphi_r^*$ for $\omega_l^* = 80$ rad/s are depicted in Fig. 22. The time history of the phase shift $\psi(t)$ is plotted in Fig. 23. As it seen from the plots, that $\psi(t)$ tends to the given value $\pi/2$ and that the prescribed phase shift is ensured with an appropriate precision. The situation is drastically changed if $\omega_l^* = 80$ rad/s is taken, see time histories in Fig. 24. Plot of $\sin\psi$ presented in Fig. 25 shows that at this frequency phase shift $\psi(t)$ does not tend to any constant value. This result is consistent with the impression obtained earlier in the work on controlled phase synchronization (Andrievsky *et al.*, 2019; Fradkov *et al.*, 2021) that the ability to control the phase shift between unbalanced rotors is limited due to their tendency to self-synchronize at high speeds. Expanding the capabilities of controlled synchronization through the use of alternative control methods is an area for further research.

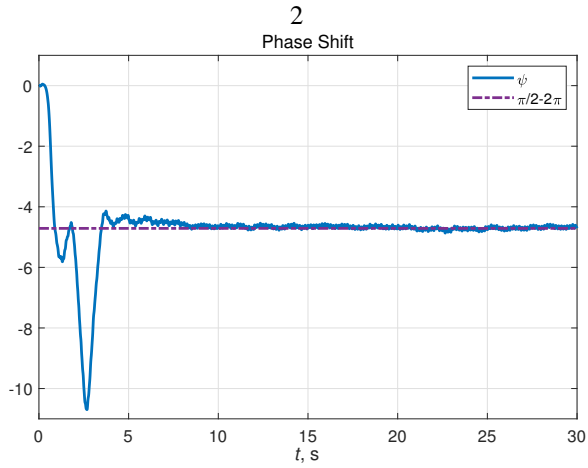

Figure 23. Time history of phase shift $\psi(t)$ for $\omega_l^* = 80$ rad/s, $\kappa = 2, \psi^* = \pi/2$.

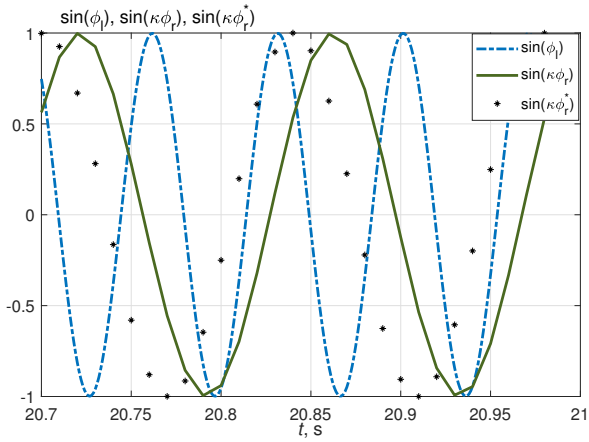

Figure 24. Time histories of $\sin\varphi_l$, $\sin\varphi_r$ and desired process $\sin\varphi_r^*$ for $\omega_l^* = 90$ rad/s, $\kappa = 2, \psi^* = \pi/2$.

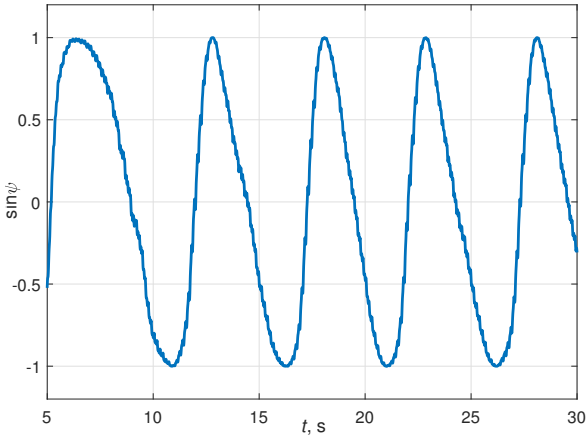

Figure 25. Time history of $\sin\psi(t)$ for $\omega_l^* = 90$ rad/s, $\kappa = 2$, $\psi^* = \pi/2$.

The existing phase self-synhronization phenomenon is studied experimentally. To this end, $\omega_r^* = \omega_l^* = \omega^*$ were set, phase PI-controller (7) in (1)–(8) was excluded and the following control algorithm was used indtead:

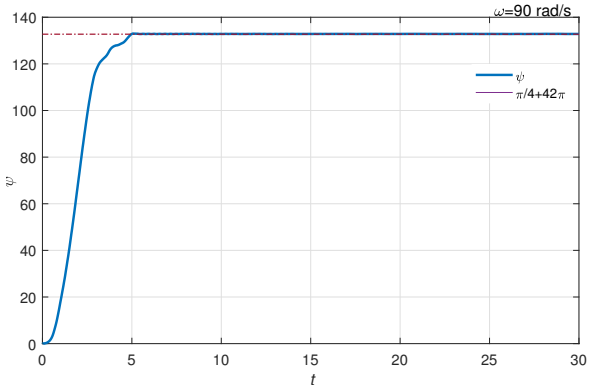

Figure 26. Time history of phase shift $\psi(t)$. Self-synchronization in phase for control law (15)–(17) at $\omega_r^* = \omega_l^* = 90$ rad/s.

$$e_{\omega_l} = \omega_l^* - \omega_l, \quad e_{\omega_r} = \omega_r^* - \omega_r, \tag{15}$$

$$\dot\sigma_{\omega l} = e_{\omega_l}, \quad u_l = K_{i\omega_l}\sigma_{\omega l} + K_{p\omega_l}e_{\omega_l}, \tag{16}$$

$$\dot\sigma_{\omega r} = e_{\omega_r}, \quad u_r = K_{i\omega_r}\sigma_{\omega r} + K_p e_{\omega_r}, \tag{17}$$

see (1)–(8) for the definitions.

Time history of phase shift $\psi(t)$ for $\omega_r^* = \omega_l^* = 90$ rad/s is plotted in Fig. 26, confirming presence of the self-synchronization in phase for high frequencies. The plot shows that the steady-state phase shift between the rotors is very close to $\pi/4$ radians (accurate to whole revolutions).

6 Conclusions

In the paper the problem of multiple controlled synchronization of a pair of unbalanced rotors is considered. To solve it, the new bidirectional control law, employing three PI-controllers with the cross-coupling is proposed. A linear analysis of the dynamics of a simplified system is presented, demonstrating the robustness of the control system with respect to the parameters of the vibration machine and the controller. The experimental results obtained at the MMLS SV-2M of the IPME RAS are presented, demonstrating the efficiency of the proposed approachIt shown that in a certain range of middle frequencies, a given normalized phase shift between unbalanced rotors rotating with multiple frequencies can be provided by the proposed control law, and the resulting behavior will be stable and robust with respect to parameters of the mechanical system and controller. It was also obtained that the ability to control the phase shift between unbalanced rotors at high frequencies is limited due to the tendency for self-synchronization of the rotors.

Expanding the capabilities of controlled synchronization through the use of unidirectional (master-slave synchronization) and alternative control methods, such

as adaptive, sliding mode, Speed gradient, Neural Networks, as well nonlinear correction methods is an area for further research. It is also planned to perform the investigations on ensuring the specified characteristics of the movement of vibrating platforms (the so called "vibration fields") due to multiple synchronization with a controlled phase shift and to study the possibility of chaotization in this way for improvement the bulk materials mixing.

Acknowledgment

The paper is dedicated to the blessed memory of Professor Ilya Izrailevich Blekhman, who opened the prospects for investigations on vibration phenomena and their applications to science and technology for many researches both in Russia and the worldwide.

This work was supported by the Ministry of Science and Higher Education of the Russian Federation (Project No. 075-15-2021-573).

References

Andrievskii, B. R., I. I. Blekhman, L. I. Blekhman, V. I. Boikov, V. B. Vasil'kov and A. L. Fradkov (2016). Education and research mechatronic complex for studying vibration devices and processes. *J. Mach. Manuf. Reliab.* **45**(4), pp. 369–374. (translated from original Russian text published in Problemy Mashinostroeniya i Nadezhnosti Mashin, 2016, No. 4, pp. 91–97).

Andrievsky, B., A.L. Fradkov, O.P. Tomchina and V.I. Boikov (2019). Angular velocity and phase shift control of mechatronic vibrational setup. *IFAC-PapersOnLine* **52**(15), pp. 436–441.

Andrievsky, B. and V. I. Boikov (2017). Experimental study of multiresonance mechatronic vibrational laboratory set-up. *Cybernetics and Physics* **5**(1), pp. 5–11.

Andrievsky, B. R., A. A. Stotsky and A. L. Fradkov (1989). Velocity gradient algorithms in control and adaptation problems. *Autom. Remote Control* pp. 1533–1564.

Andrievsky, B., V. I. Boikov, A. L. Fradkov and R. E. Seifullaev (2016). Mechatronic laboratory setup for study of controlled nonlinear vibrations. *IFAC-PapersOnLine* **49**(14), 1–6. 6th IFAC Workshop on Periodic Control Systems PSYCO 2016.

Blekhman, I. (2012). Oscillatory strobodynamics – A new area in nonlinear oscillations theory, nonlinear dynamics and cybernetical physics. *Cybernetics and Physics* **1**(1), pp. 5–10.

Blekhman, I. I. (1988). *Synchronization in science and technology*. ASME Press. New-York.

Blekhman, I. I. (2000). *Vibrational Mechanics: Nonlinear Dynamic Effects, General Approach, Applications*. World Scientific. Singapore.

Blekhman, I. I. (2013). *Teoriya vibracionnyh processov i ustrojstv. Vibracionnaya mekhanika i vibracionnaya tekhnika (The theory of vibration processes and devices. Vibrational mechanics and vibrational engineering)*. Publishing house "Ruda i metally". St. Petersburg. (in Russian).

Blekhman, I. I., A. L. Fradkov, H. Nijmeijer and A. Y. Pogromsky (1997). On self-synchronization and controlled synchronization of dynamical systems. *Systems & Control Letters* **31**(5), pp. 299–306.

Blekhman, I. I., A. L. Fradkov, O. P. Tomchina and D. E. Bogdanov (2002). Self-synchronization and controlled synchronization: General definition and example design. *Mathematics and Computers in Simulation* **58**(4–6), pp. 367–384.

Blekhman, I. I. and L. A. Vaisberg (2011). Self-synchronization as a self-organization phenomenon and a basis for development of energy-efficient technologies. In: *Proc. 10th Biennial International Conference on Vibration Problems (ICOVP)* (S. Segla, J. Tuma and I. Petrikova, Eds.). Prague, Czech Republic. pp. 365–370.

Blekhman, I. I. and N. P. Yaroshevich (2004). Extension of the domain of applicability of the integral stability criterion (extremum property) in synchronization problems. *J. Applied Mathematics and Mechanics*.

Blekhman, I. I., P. S. Landa and M. G. Rosenblum (1995). Synchronization and chaotization in interacting dynamical systems. *Applied Mechanics Reviews* **48**(11), pp. 733–752.

Blekhman, I.I. and A.L. Fradkov (2004). On general definitions of synchronization. In: *Selected Topics in Vibrational Mechanics* (I. I. Blekhman, Ed.). pp. 179–188. World Scientific. Singapore.

Boikov, V. I., B. Andrievsky and V. V. Shiegin (2016). Experimental study of unbalanced rotors synchronization of the mechatronic vibration setup. *Cybernetics and Physics* **5**(1), pp. 5–11.

Bucolo, M., A. Buscarino, L. Fortuna and M. Frasca (2022). Nyquist plots for MIMO systems under frequency transformations. *IEEE Control Systems Letters* **6**, pp. 169–174.

Cvetićanin, L. and M. Zukovic (2015). Non-ideal mechanical system with an oscillator with rational nonlinearity. *J. Vibration and Control* **21**(11), pp. 2149–2164.

Dimentberg, M. F., L. McGovern, R. L. Norton, J. Chapdelaine and R. Harrison (1997). Dynamics of an unbalanced shaft interacting with a limited power supply. *Nonlinear Dynamics* **13**, pp. 171–187.

Fradkov, A. L. (1979). Speed-gradient scheme and its applications in adaptive control. *Autom. Remote Control* **40**(9), pp. 1333–1342.

Fradkov, A. L. and A. Yu. Pogromsky (1998). *Introduction to control of oscillations and chaos*. World Scientific Publishers. Singapore.

Fradkov, A. L., I. V. Miroshnik and V. O. Nikiforov (1999). *Nonlinear and Adaptive Control of Complex Systems*. Kluwer. Dordrecht.

Fradkov, A.L., D. Gorlatov, O. Tomchina and D. Tomchin (2016). Control of oscillations in vibration machines: Start up and passage through resonance. *Chaos* **26**(11), 116310.

Fradkov, A.L., O. Tomchina, V. Galitskaya and D. Gorlatov (2013). Multiple controlled synchronization for 3-rotor vibration unit with varying payload. *IFAC-PapersOnLine* **46**(12), pp. 5–10.

Fradkov, A.L, O.P. Tomchina and D.A. Tomchin (2011). Controlled passage through resonance in mechanical systems. *J. Sound and Vibration* **330**(6), pp. 1065–1073.

Fradkov, A.L., O.P. Tomchina, B. Andrievsky and V.I. Boikov (2021). Control of phase shift in two-rotor vibration units. *IEEE Trans. Control Syst. Technol.* **29**(3), pp. 1316–1323.

Galitskaya, V.A. and O.P. Tomchina (2012). Proportsional'no-integral'nyy energoskorostnoy algoritm upravleniya kratnoy sinkhronizatsiyey rotorov vibratsionnoy ustanovki [Proportional-integral energy-speed control algorithm for multiple synchronization of rotors of a vibration setup]. *Informatika i sistemy upravleniya* (3 (33)), pp. 158–168. (in Russian).

Giri, F., Ed.) (2013). *AC Electric Motors Control: Advanced Design Techniques and Applications*. John Wiley & Sons, Ltd. Chichester, UK.

Gorlatov, D. V., D. A. Tomchin and O. P. Tomchina (2015). Controlled passage through resonance for two-rotor vibration unit: Influence of drive dynamics. In: *Proc. 1st IFAC Conference on Modelling, Identification and Control of Nonlinear Systems (MICNON 2015), IFAC-PapersOnLine*. Vol. 48 (11). pp. 313–318. IFAC. Saint Petersburg, Russia.

He, F., W. Tong and Q. Wang (2007). Synchronization control strategy of multi-motor system based on profibus network. In: *2007 IEEE Intern. Conf. Automation and Logistics*. pp. 3029–3034.

Jia, L., X. Kong, J. Zhang, Y. Liu and B. Wen (2018). Multiple-frequency controlled synchronization of two homodromy eccentric rotors in a vibratory system. *Shock and Vibration* **2018**, pp. 1–12.

Joshi, B.M. and M.C. Chandorkar (2014). Two-motor single-inverter field-oriented induction machine drive dynamic performance. *Sadhana* **39**(2), pp. 391–407.

Khalil, H. K., E. G. Strangas and S. Jurkovic (2009). Speed observer and reduced nonlinear model for sensorless control of induction motors. *IEEE Trans. Control Syst. Technol.* **17**, pp. 327 – 339.

Kovriguine, D. A. (2012). Synchronization and Sommerfeld effect as typical resonant patterns. *Arch. Appl. Mech.* **82**, pp. 591–604.

Kremer, E. (2016). Slow motions in systems with fast modulated excitation. *J. Sound and Vibration* **383**, pp. 295–308.

Li, L. and X. Chen (2019). Multi-frequency vibration synchronization and stability of the nonlinear screening system. *IEEE Access* **7**, pp. 171032–171045.

Liu, Y., X. Zhang, D. Gu, L. Jia and B. Wen (2020). Synchronization of a dual-mass vibrating system with two exciters. *Shock and Vibration* **2020**, pp. 1–12.

Ljung, L. (1999). *System Identification: Theory for the User*. Prentice Hall. Upper Saddle River, NJ, USA. 2nd Ed.

Sommerfeld, A. (1902). Beitrage zum dynamischen ausbau der festigkeislehre. *Z. Ver. Deut. Ing.* **46**, pp. 391–394. (in German).

Tomchin, D. A. and A. L. Fradkov (2005). Controlling passage of a rotor through the resonance band by the velocity-gradient method. *J. Machinery Manufacture and Reliability* **5**, pp. 55–60.

Tomchina, O. (2018). Control of vibrational field in a cyber-physical vibration unit. *Cybernetics and Physics* **7**(3), pp. 144–151.

Tomchina, O. (2020). Control of oscillations in two-rotor cyberphysical vibration units with time-varying observer. *Cybernetics and Physics* **9**(4), pp. 206–213.

Tomchina, O. P., I. M. Kudryavtseva and V. A. Galitskaya (2009). Algoritmy upravleniya kratnoy sinkhronizatsiyey dlya dvukhrotornykh vibratsionnykh ustanovok [Multiple Synchronization Control Algorithms for Two-Rotary Vibration Setups]. In: *Nelineynyye problemy teorii kolebaniy i teorii upravleniya. Vibratsionnaya mekhanika [Nonlinear problems of oscillation theory and control theory. Vibration Mechanics]* (V. V. Beletsky, D. A. Indeytsev and A. L. Fradkov, Eds.). pp. 455–474. Nauka. SPb. (in Russian).

Vitturi, S. (2004). On the effects of the acyclic traffic on Profibus DP networks. *Computer Standards & Interfaces* **26**(2), pp. 131–144.